

Fig. 6.1. Bound states in an infinitely deep square well. The long-dash line indicates the potential energy $V(x)$. It vanishes for $-d/2 < x < d/2$ and is infinite elsewhere. Points $x = \pm d/2$ are indicated as vertical walls. On the left side an energy scale is drawn, and to the right of it the energies E_n of the lower-lying bound states are indicated by horizontal lines. These lines are repeated as short-dash lines on the left. They serve as zero lines for the wave functions $\varphi(x)$ and the probability densities $|\varphi(x)|^2$ of the bound states.

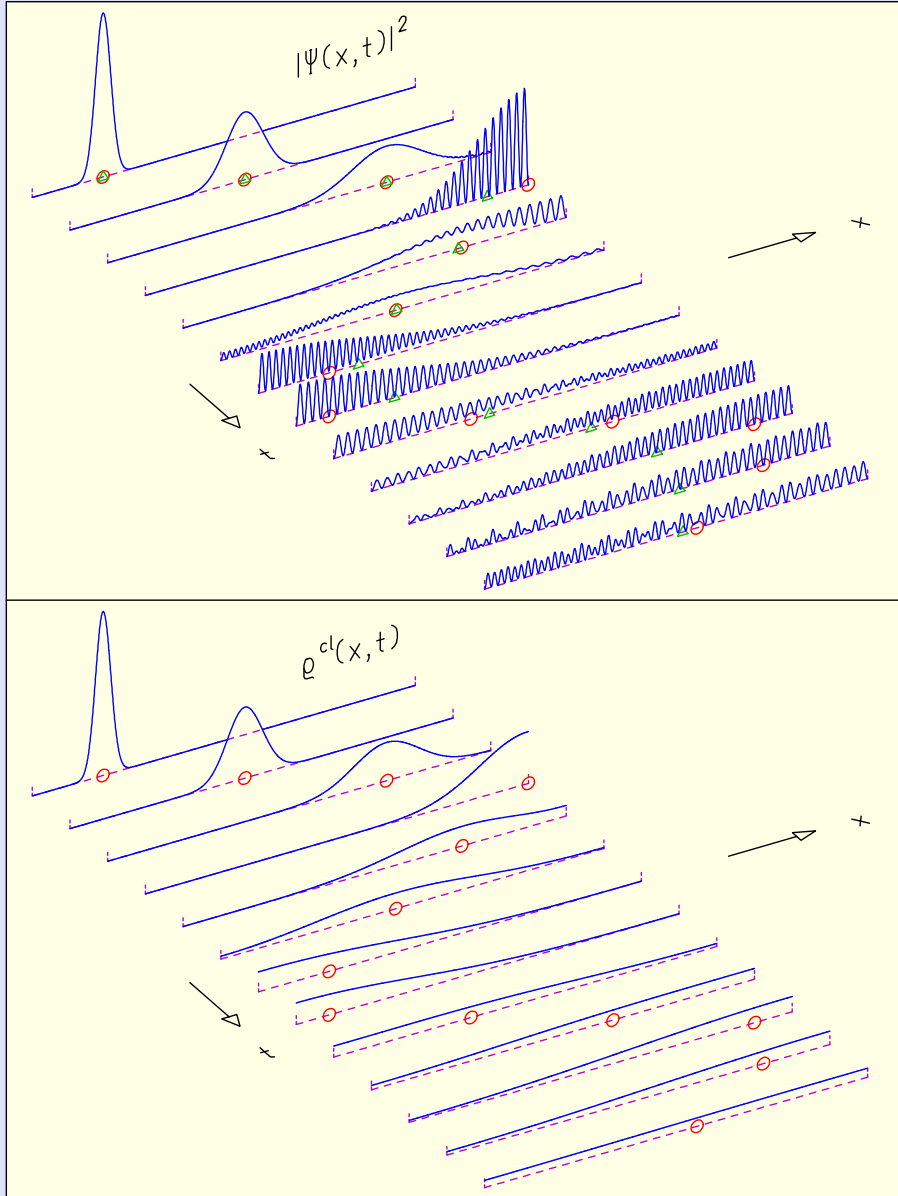


Fig. 6.2. Top: Time development of a wave packet moving in an infinitely deep square well. At $t = 0$, in the background, the smooth packet is well concentrated. Its initial momentum makes it bounce back and forth between the two walls. The characteristic interference pattern of the reflection process, as well as the dispersion of the packet with time, is apparent. The small circle indicates the position of the corresponding classical particle. The quantum-mechanical position expectation value is shown by a small triangle. Bottom: Time development of the spatial probability density computed from the classical phase-space distribution corresponding to the quantum-mechanical wave packet.

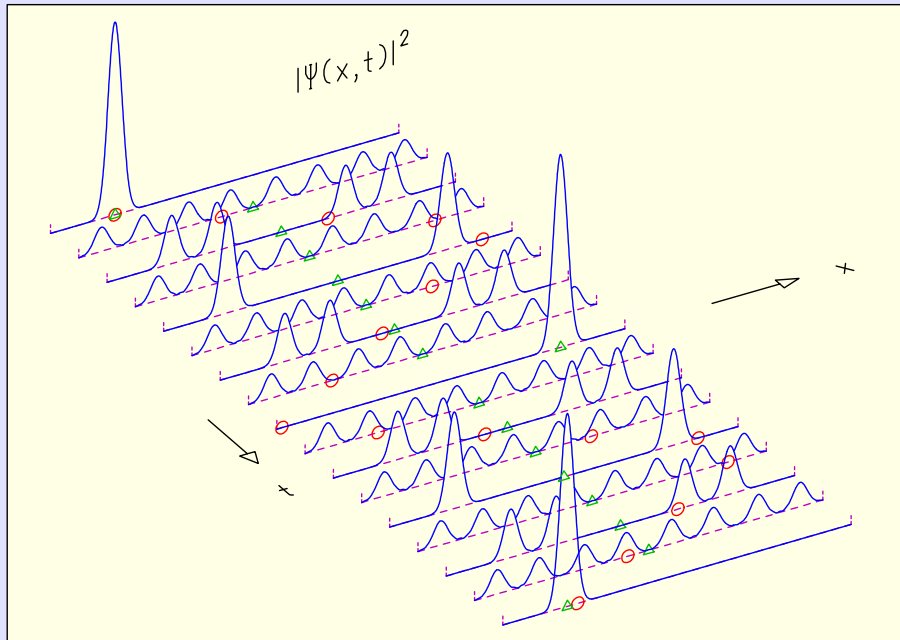


Fig. 6.3. Time development of the same wave packet as in Figure 6.2 but observed of a full revival period T_1 . The time interval shown in Figure 6.2 is $T_1/60$.

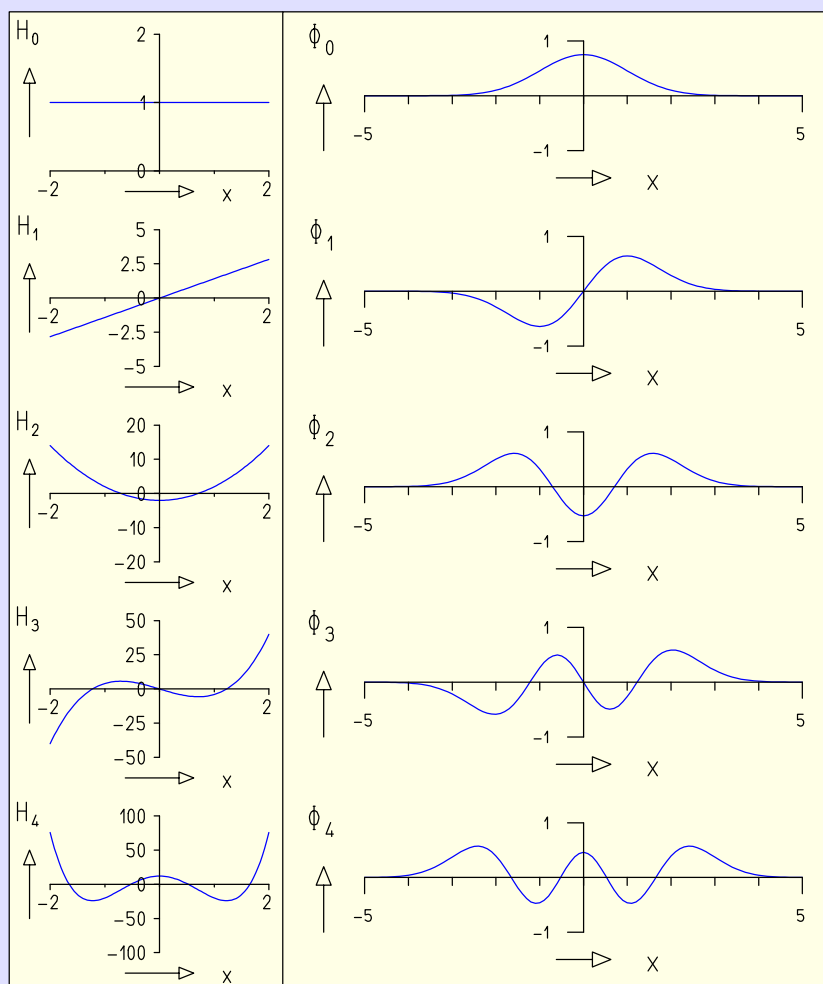


Fig. 6.4. Hermite polynomials $H_n(x)$ and eigenfunctions $\phi_n(x)$ of the harmonic oscillator for low values of n .

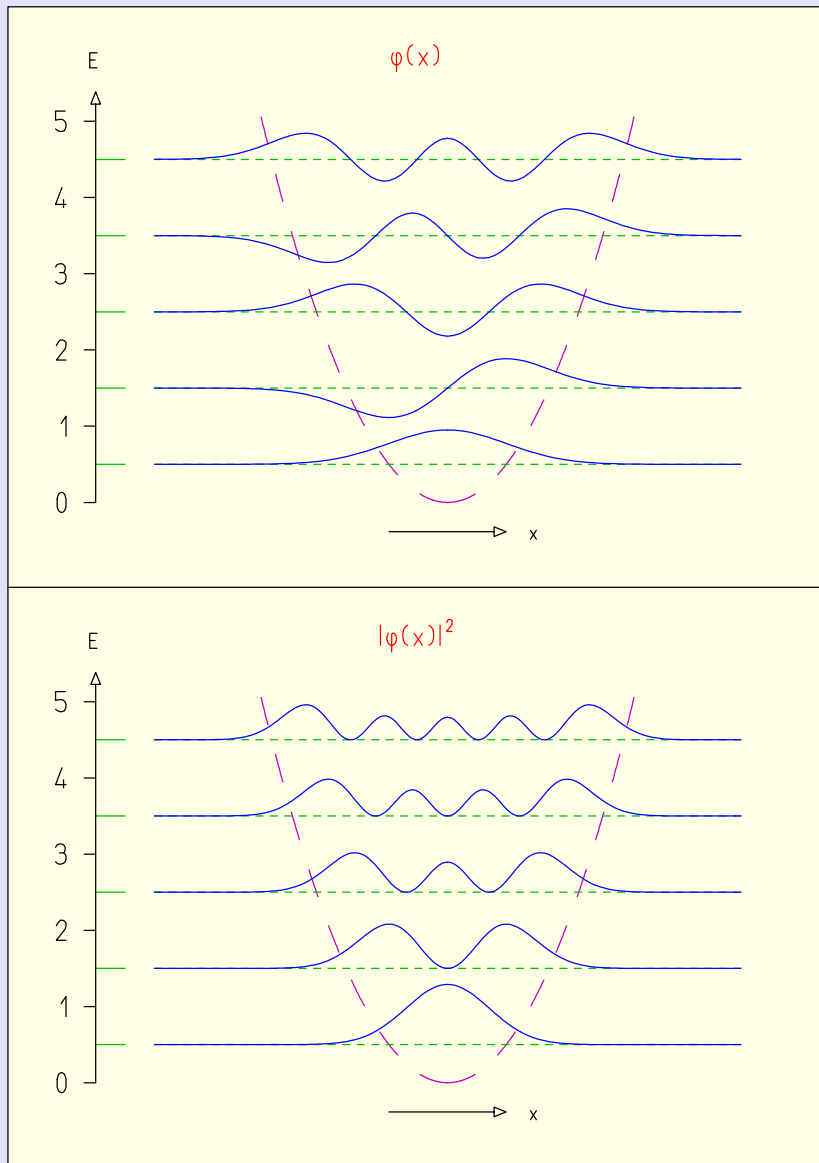


Fig. 6.5. Bound states in a harmonic-oscillator potential. The potential is drawn as a long-dash line, a parabola. The eigenvalue spectrum of bound states (in units of $\hbar\omega$) is indicated by the horizontal lines on the left side. Repeated on the right as short-dash lines, they serve as zero lines for the wave functions $\varphi(x)$ and the probability densities $|\varphi(x)|^2$ of the bound states.

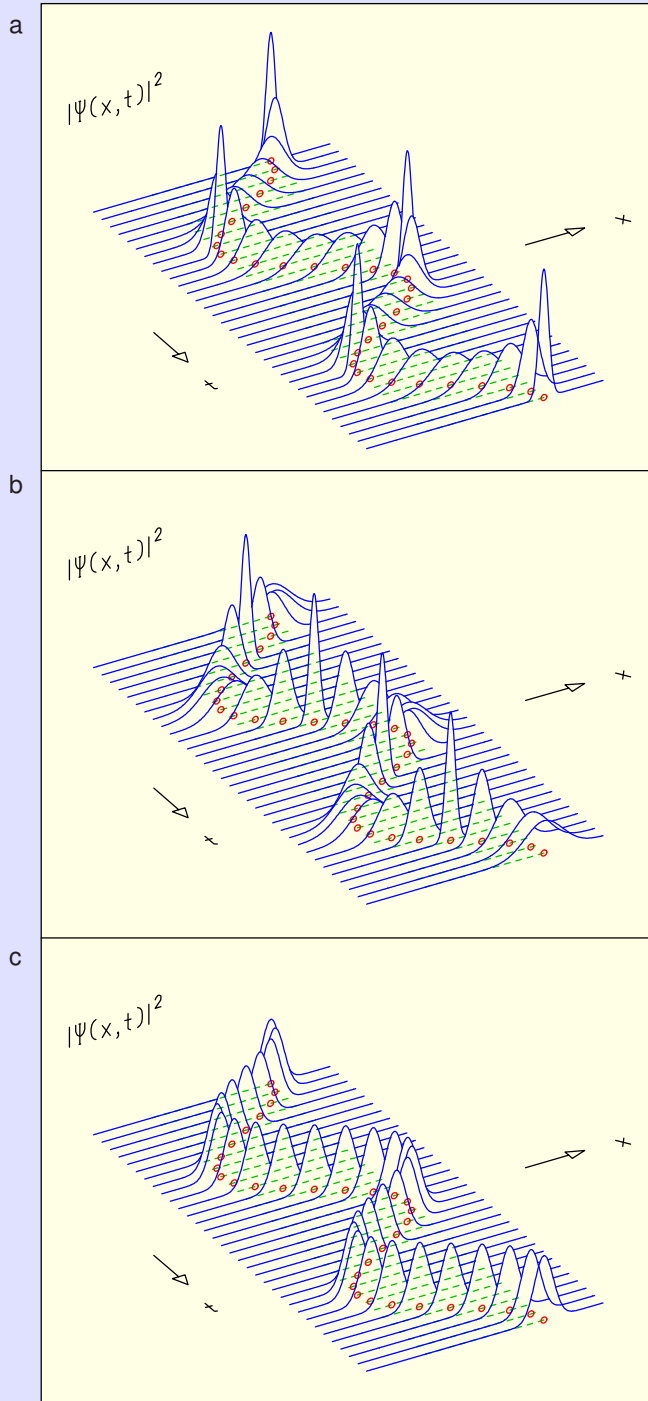


Fig. 6.6. Time development of a Gaussian wave packet, represented by its probability density, under the influence of a harmonic force. The circles show the motion of the corresponding classical particle. The broken lines extend between its turning points. The wave packet is initially at rest at an off-center position. (a) The initial width of the wave packet is smaller than that of the oscillator's ground state. (b) The initial width of the wave packet is greater. (c) Both widths are equal.

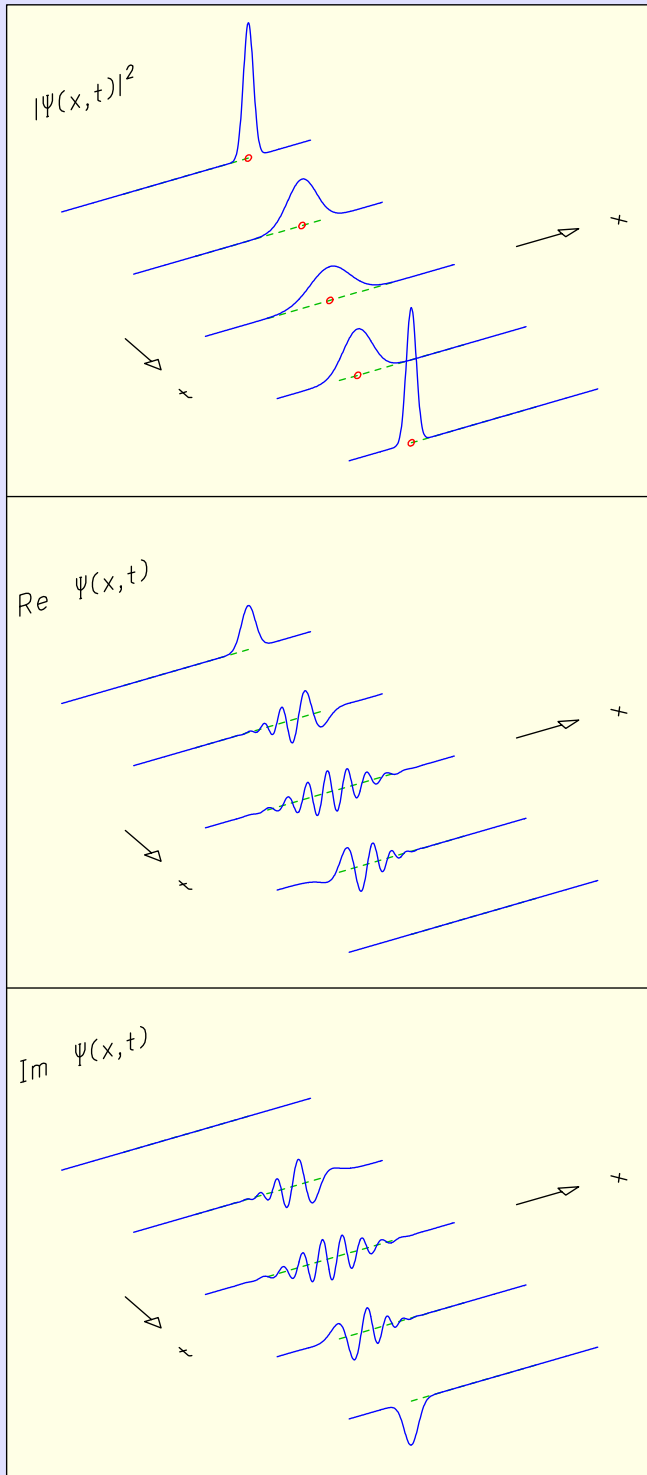


Fig. 6.7. Time development of a Gaussian wave packet under the influence of a harmonic force, observed over half an oscillation period. Shown are the probability density, the real part of the wave function, and the imaginary part of the wave function.

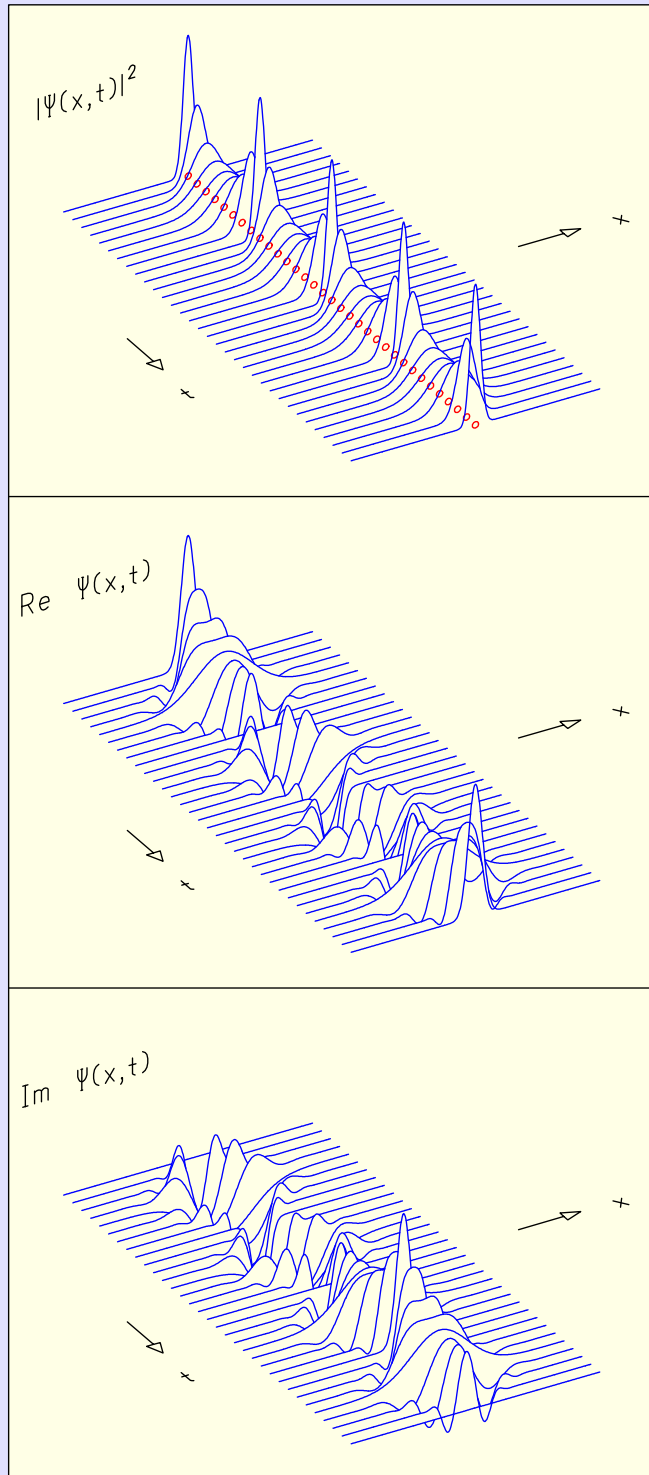


Fig. 6.8. Time development of a wave packet at rest in the center of a harmonic oscillator. The packet is represented by its probability density, and by the real part, and the imaginary part of its wave function. Since its initial width is different from that of the oscillator's ground state, the width of the packet oscillates in time with twice the oscillator frequency. Except for the initial position, all parameters are identical to those of Figure 6.7.

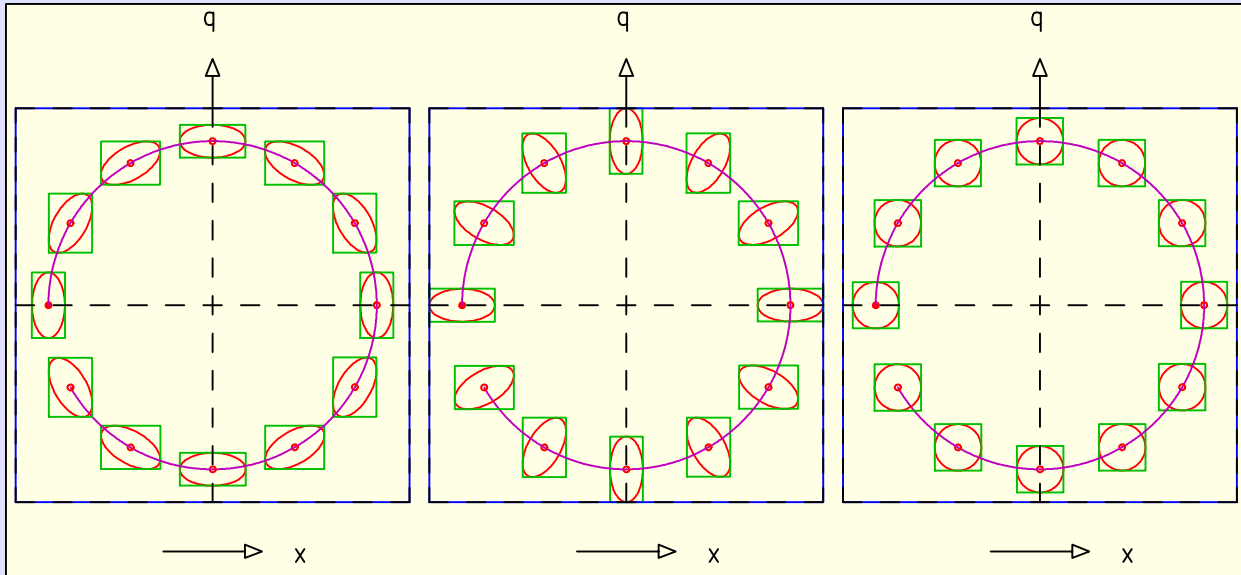


Fig. 6.9. Motion of the covariance ellipse of a classical phase-space density under the influence of a harmonic force. The large circle is the trajectory of the center of the ellipse. The ellipse is shown for equidistant moments in time. The rectangle circumscribing it has sides σ_x , σ_q . The small circles indicate the centers of the ellipses. For the initial time it is drawn as a full dot. The relation between the initial widths is (left) $\sigma_{x0} < \sigma_{q0}$, (middle) $\sigma_{x0} > \sigma_{q0}$, and (right) $\sigma_{x0} = \sigma_{q0}$.

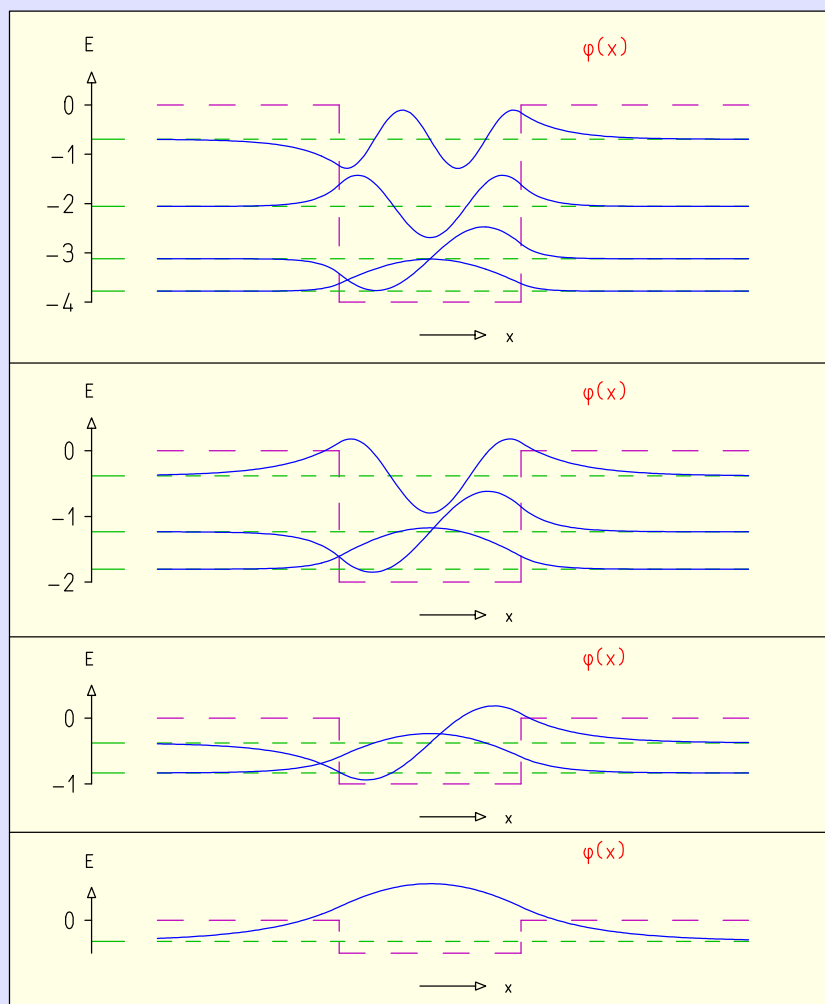


Fig. 6.10. Bound-state wave functions and energy spectra for square-well potentials of different finite depths but identical widths. The number of bound states increases with the depth of the potential.

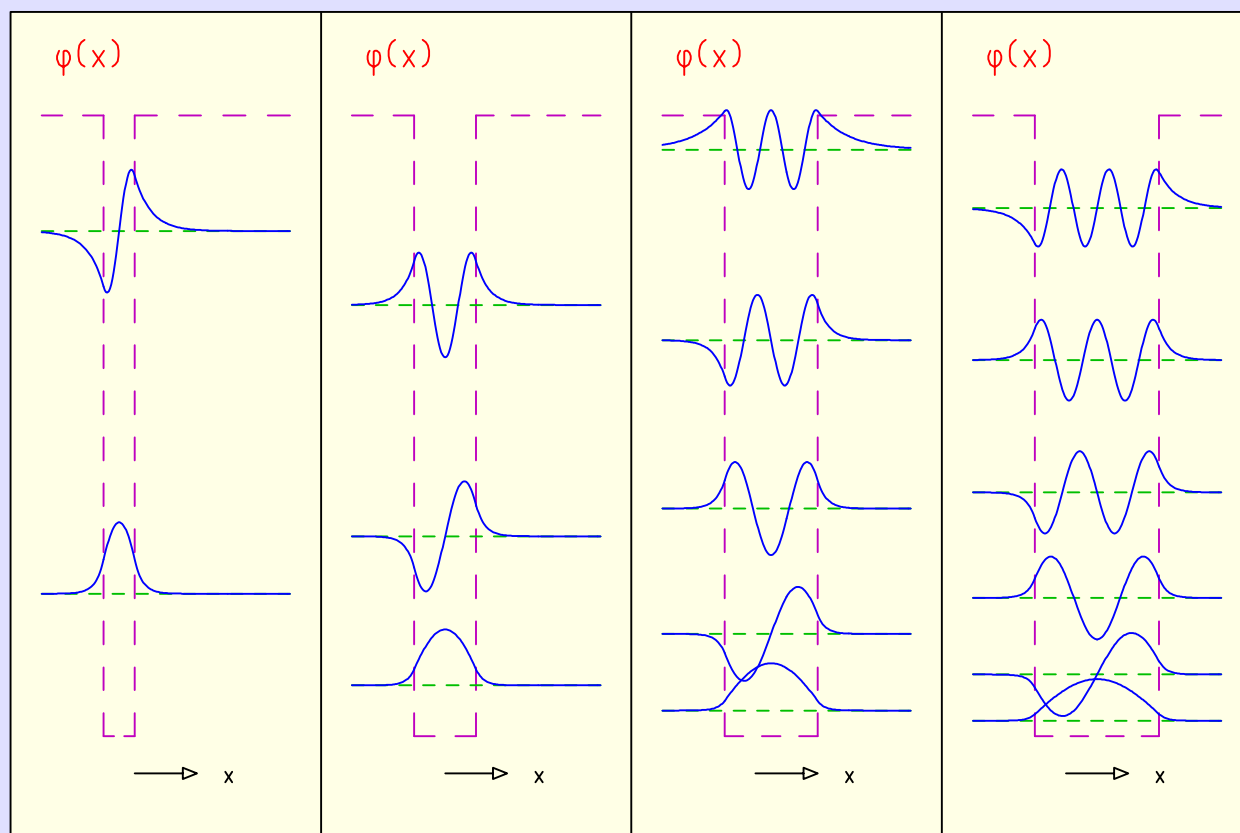


Fig. 6.11. Bound-state wave functions for square-well potentials of identical depth but different widths. The number of bound states increases with the width of the well.

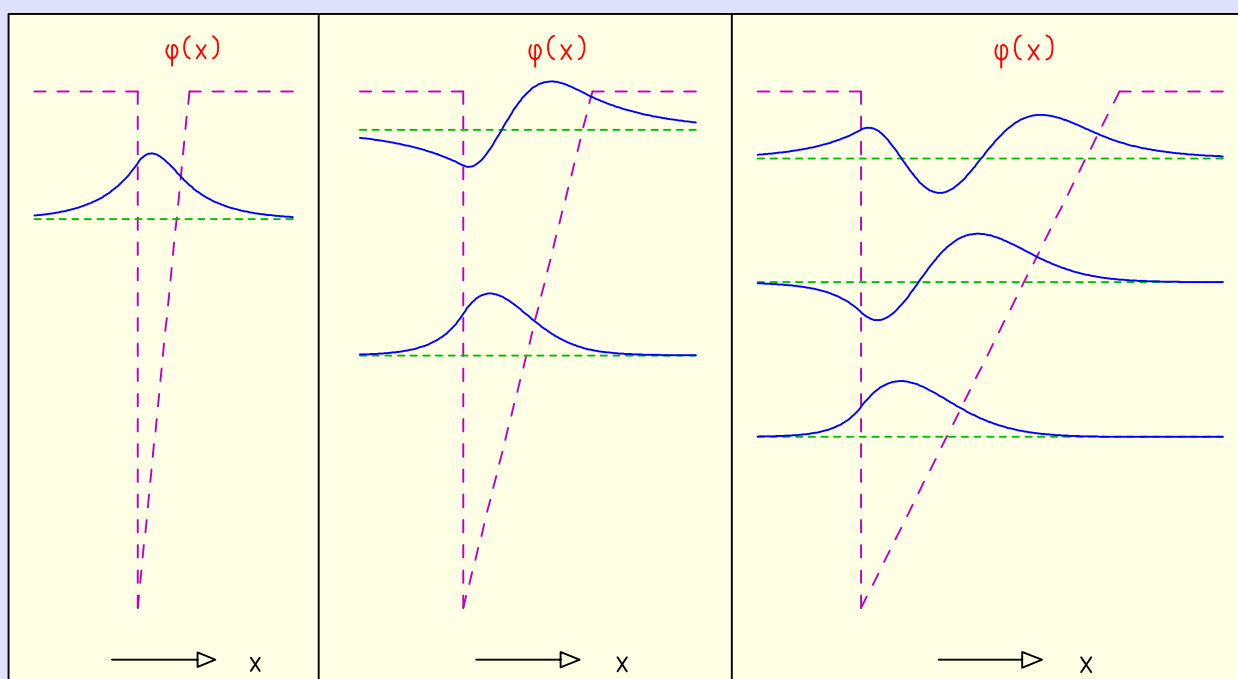


Fig. 6.12. Bound-state wave functions for skew triangular potential wells of identical depth but different opening angles. The number of bound states increases with the opening of the well.

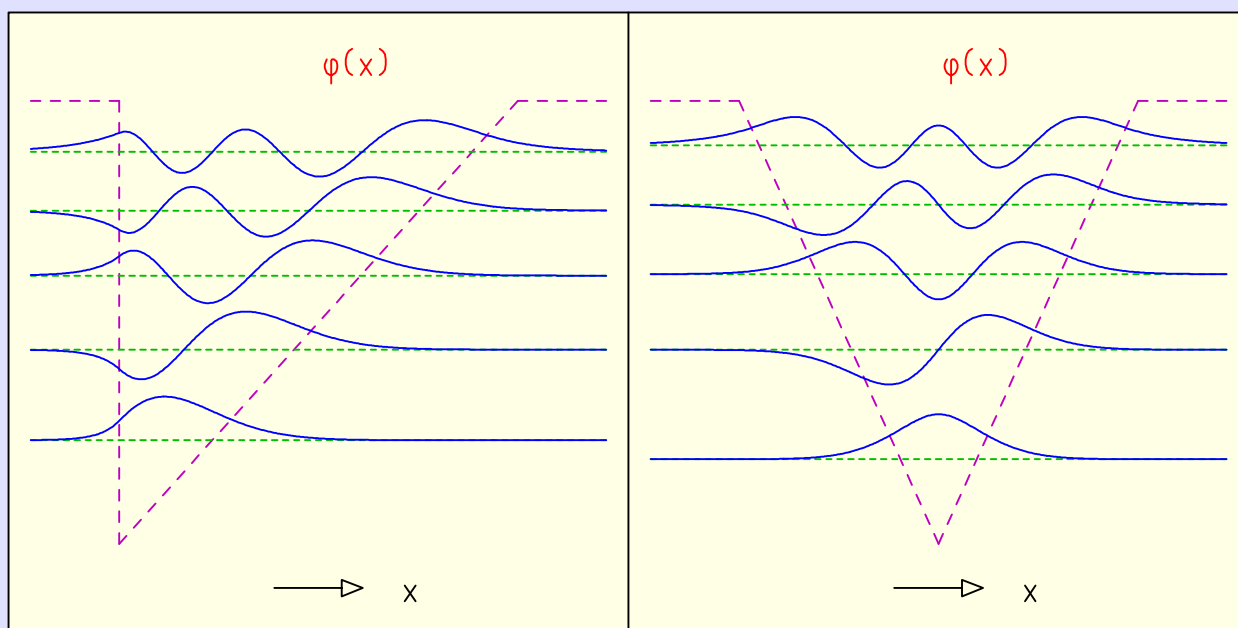


Fig. 6.13. Bound-state wave functions for a skew and for a symmetric triangular potential well. Both are equally wide at the top. In the symmetric potential the lowest state is lower and the highest state is higher than in the skew potential.

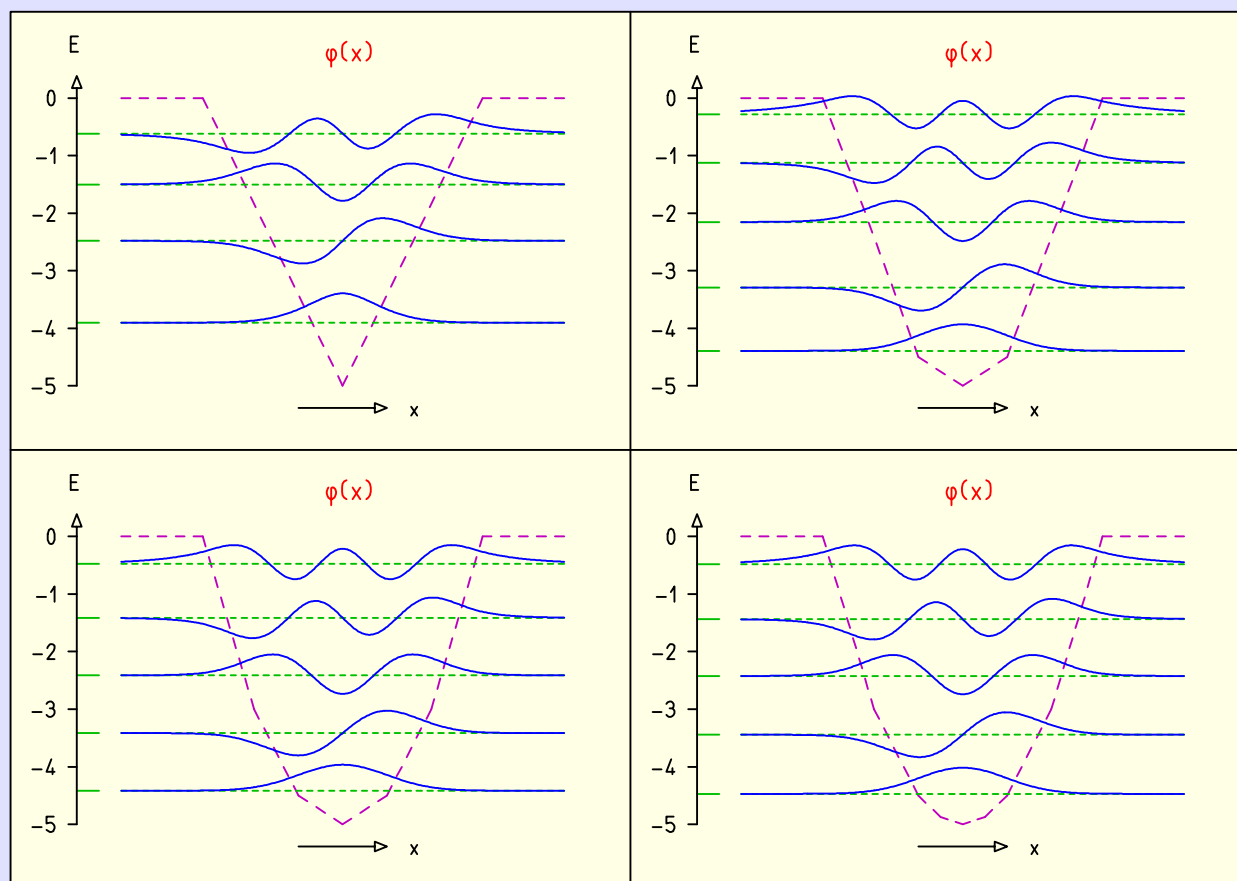


Fig. 6.14. Successive approximation of the harmonic-oscillator potential of Fig. 6.5 by a piecewise linear potential.

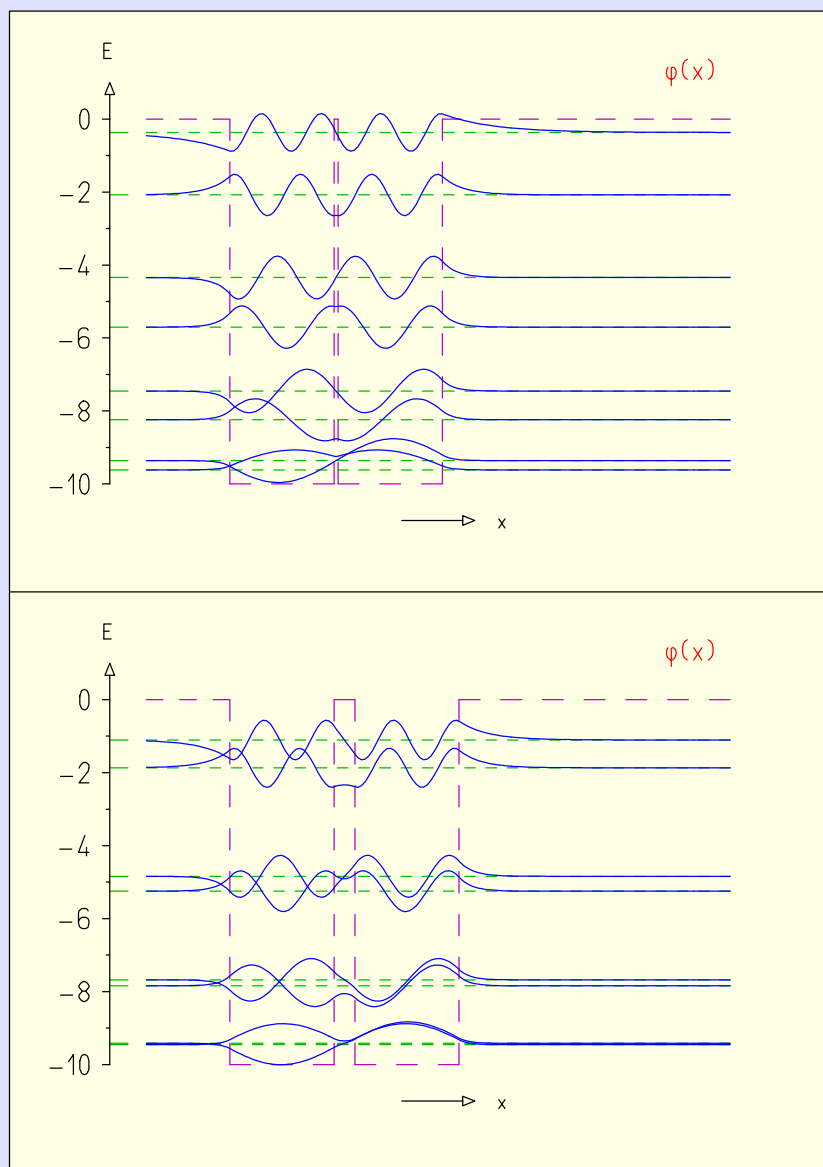


Fig. 6.15. Bound-state wave functions and energy spectra for systems of two square wells. In one system the wells are very close together, in the other some distance apart.

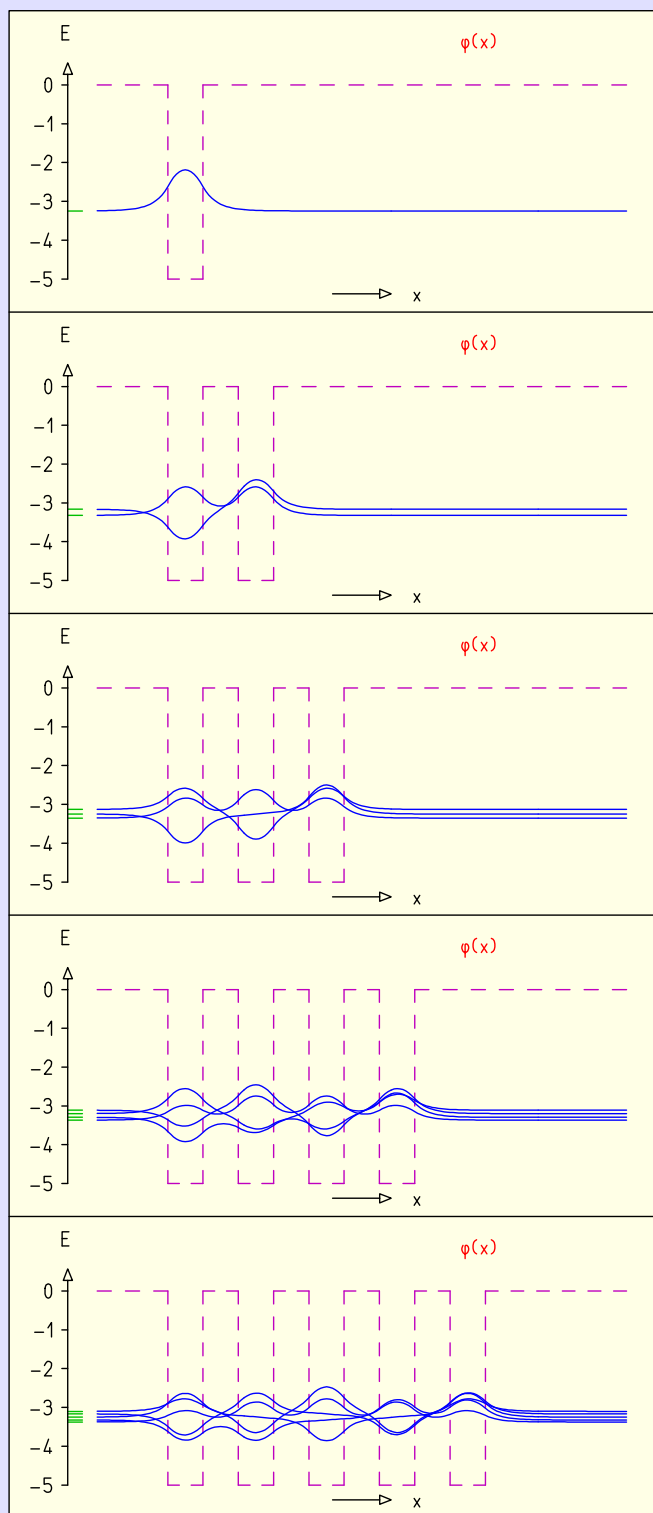


Fig. 6.16. Bound-state wave functions and energy spectra for a potential well and for potentials consisting of two, three, four, and five neighboring wells. The states have very similar energies.

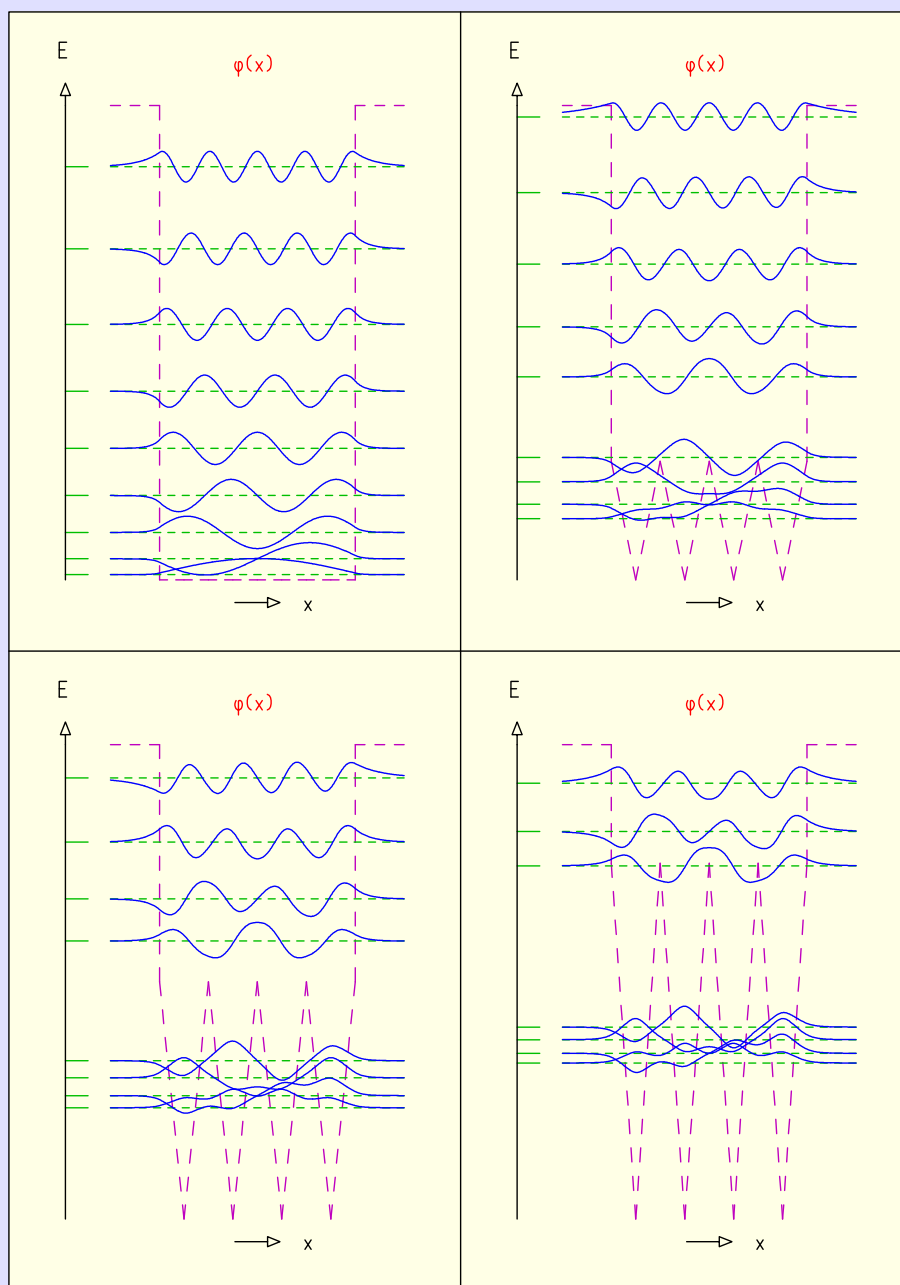


Fig. 6.17. The square well (top left) is gradually transformed into a quasiperiodic potential with four wells. As a result the lowest four bound states form a band with closely spaced energies.